

Thermal convection in a linearly viscous fluid overlying a bidisperse porous medium

P. Dondl

Abteilung für Angewandte Mathematik
Albert-Ludwigs-Universität Freiburg
Hermann-Herder-Str. 10,
79104 Freiburg, Germany

and

B. Straughan

Department of Mathematics
University of Durham, Durham DH1 3LE, UK

October 26, 2021

Abstract

A bidisperse porous medium is one with two porosity scales. There are the usual pores known as macro pores but also cracks or fissures in the skeleton which give rise to micro pores. In this article we develop and analyse a model for thermal convection where a layer of viscous incompressible fluid overlies a layer of bidisperse porous medium. Care has to be taken with the boundary conditions at the interface of the fluid and the porous material and this aspect is investigated. The situation is one in a layer which is heated from below and under appropriate conditions bimodal neutral curves are found. These depend on the ratio \hat{d} of the depth d of the fluid layer to the depth d_m of the porous layer. We show that there is a critical value of \hat{d} such that below this value convective motion initiates in the porous layer whereas for \hat{d} above this value the convective instability commences in the fluid layer.

1 Introduction

The problem of flow of a fluid overlying a porous medium saturated by the same fluid is one which has attracted the attention of many prominent scientists. A fundamental interface condition between the fluid and the porous medium was proposed by Beavers and Joseph [2]. The first analysis of thermal convection in the situation where a fluid overlies a saturated porous medium is due to

Nield [38] who successfully employed the Beavers - Joseph boundary condition to derive a satisfactory model. A surprising result for the same thermal convection problem was discovered by Chen and Chen [14] who showed that the ratio of fluid depth, d , to porous layer depth, d_m , defined by $\hat{d} = d/d_m$, is critical to determining the process for the onset of thermal convection in the two layer system. If \hat{d} is below a critical value then convection commences in the porous layer whereas when \hat{d} is above the critical value then convection commences in the fluid. This class of problem was further investigated both experimentally and theoretically by Chen and Chen [15, 16], Chen [13], McKay and Straughan [36], where the last mentioned article applies the theory to the problem of stone formation into regular patterns at the bottom of a shallow lake.

The subject of thermal convection or generally flow in a two layer system has been studied in much detail with a review of the early work and applications to various areas in industry or geophysics given in chapter 6 of Straughan [50]. The intense interest in this class of problem has been driven by the many applications to diverse areas such as heat pipe technology, renewable energy, see e.g. Straughan [50], contaminant dispersal in water ways, Hibi and Tomigashi [25], Hibi [24], or even blood flow in arteries and veins in the human body, see e.g. Sharma and Yadav [47], Tiwari et al. [55], Ponalagusamy and Manchi [42], Wajihah and Sankar [57]. Indeed, the last mentioned article involves 5 layer flow comprising Darcy media, Brinkman media, plasma, core flow, and plug flow.

There are many recent stability analyses of fluid flow in the two layer fluid - porous configuration, see e.g. Carr and Straughan [8], Chang et al. [11], Hill and Straughan [26, 28], Chang et al. [12], Samanta [45], Yin et al. [60], Tsiberkin [56]. Particular analyses involving the nonlinear theory and bifurcations are given by Han et al. [23], McCurdy et al. [35], Lyu and Wang [34], and Hill and Straughan [27]. In addition, mathematical analysis of the structural stability of the two layer system has been thoroughly investigated, see e.g. Li et al. [31], Li et al. [33], Li et al. [32], Payne and Straughan [41].

In a separate development, there has been immense interest in thermal convection in a single layer of saturated porous material but when the porous skeleton is of double porosity type. By double porosity we mean that the solid skeleton contains pores of a visible size known as macro pores, but the skeleton itself contains cracks or fissures which give rise to much smaller micropores. Flow in such materials is additionally called bidisperse or bidispersive. The thermal convection problem in a bidisperse porous material was first developed by Nield and Kuznetsov [40] who allowed for different velocities, pressures and temperature fields in the macro and micro phases and a critical review of the topic is given by Gentile and Straughan [22]. There are many recent contributions driven by the need to understand bidispersive convection in real life applications, cf. Gentile and Straughan [22], Straughan [51], chapter 13. Analyses of bidispersive thermal convection in isotropic, anisotropic, vertical layer, inclined layer, and with rotation effects are given by Badday and Harfash [1], Capone et al. [6], Capone et al. [5], Capone and De Luca [3], Capone and Massa [4], Capone et al. [7], Chalooob et al. [9], Falsaperla et al. [18], Gentile and

Straughan [20, 21], Saravanan and Vigneshwaran [46], Straughan [52, 54, 53], and the structural stability aspect of the system of equations is considered by Franchi et al. [19].

The object of the current work is to present a model for thermal convection in an incompressible viscous fluid when that fluid overlies a bidisperse porous medium saturated with the same fluid. We analyse the instability of thermal convection in this system and show there are definite relations between the onset of convective motion and the respective depths of the fluid and porous layers, and of the properties of the macro and micro pores. This is the first analysis we have seen of this problem and we believe it has much future application to diverse areas such as blood flow, heat transfer, and renewable energy.

2 Basic equations

We suppose a linearly viscous incompressible fluid is contained in the infinite layer $\mathbb{R}^2 \times \{0 < z < d\}$ and below this is a bidisperse porous medium saturated with the same fluid and this occupies the infinite layer $\mathbb{R}^2 \times \{-d_m < z < 0\}$, with gravity acting in the negative z -direction.

The equations for the fluid in the layer $\mathbb{R}^2 \times \{0 < z < d\}$ are then, cf. Chandrasekhar [10],

$$\begin{aligned} V_{i,t} + V_j V_{i,j} &= -\frac{1}{\rho_0} p_{,i} + \nu \Delta V_i + \gamma g k_i T, \\ V_{i,i} &= 0, \\ T_{,t} + V_i T_{,i} &= \frac{k_f}{(\rho_0 c_p)_f} \Delta T, \end{aligned} \tag{1}$$

where $V_i(\mathbf{x}, t)$ is the velocity field, $T(\mathbf{x}, t)$ is the temperature field, $p(\mathbf{x}, t)$ is the pressure field, \mathbf{x} is the spatial point in the layer, and t is time. We use indicial notation throughout in conjunction with the Einstein summation convention, so that, for example,

$$\begin{aligned} V_i T_{,i} &\equiv \sum_{i=1}^3 V_i T_{,i} \equiv V_1 \frac{\partial T}{\partial x_1} + V_2 \frac{\partial T}{\partial x_2} + V_3 \frac{\partial T}{\partial x_3} \\ &\equiv U \frac{\partial T}{\partial x} + V \frac{\partial T}{\partial y} + W \frac{\partial T}{\partial z}, \end{aligned}$$

where $\mathbf{V} = (V_1, V_2, V_3) \equiv (U, V, W)$. In equations (1) $\gamma, g, \rho_0, k_f, \nu$ and c_p are the thermal expansion coefficient of the fluid, gravity, reference density, thermal conductivity of the fluid, kinematic viscosity of the fluid, and specific heat at constant pressure of the fluid. The vector $\mathbf{k} = (0, 0, 1)$ and Δ is the Laplacian

$$\Delta = \frac{\partial^2}{\partial x^2} + \frac{\partial^2}{\partial y^2} + \frac{\partial^2}{\partial z^2}.$$

For an isotropic bidisperse porous material we suppose the macro porosity is ϕ , the micro porosity is ϵ . If we denote (U_i^f, p^f) to be the pore averaged

velocity and pressure in the macropores and (U_i^p, p^p) to be the pore averaged velocity and pressure in the micropores, then the governing equations of flow in the bidisperse porous medium may be written, cf. Gentile and Straughan [20], Straughan [52],

$$\begin{aligned}
& -\frac{\mu}{K_f} U_i^f - \zeta(U_i^f - U_i^p) - p_{,i}^f + \rho_0 \gamma k_i g T^m = 0, \\
& U_{i,i}^f = 0, \\
& -\frac{\mu}{K_p} U_i^p - \zeta(U_i^p - U_i^f) - p_{,i}^p + \rho_0 \gamma k_i g T^m = 0, \\
& U_{i,i}^p = 0, \\
& (\rho_0 c)_m T_{,t}^m + (\rho_0 c)_f (U_i^f + U_i^p) T_{,i}^m = k_m \Delta T^m,
\end{aligned} \tag{2}$$

where $T^m(\mathbf{x}, t)$ is the temperature field of the fluid in the bidisperse porous medium.

Equations (1) hold on the domain $\{(x, y) \in \mathbb{R}^2\} \times \{z \in (0, d)\} \times \{t > 0\}$ while (2) hold on the domain $\{(x, y) \in \mathbb{R}^2\} \times \{z \in (-d_m, 0)\} \times \{t > 0\}$. Equations (2) assume Darcy's law holds and a Boussinesq approximation is employed. The variable μ is the dynamic viscosity of the fluid, K_f and K_p are the macro and micro permeabilities, ζ is an interaction coefficient which represents the momentum transfer between the macro and micro phases, and $(\rho_0 c)_m$, k_m are given by

$$(\rho_0 c)_m = (1 - \phi)(1 - \epsilon)(\rho_0 c)_s + \phi(\rho_0 c)_f + \epsilon(1 - \phi)(\rho_0 c)_p,$$

and

$$k_m = (1 - \phi)(1 - \epsilon)k_s + \phi k_f + \epsilon(1 - \phi)k_p,$$

where s , f and p denote values in the solid skeleton, the fluid in the macropores, and the fluid in the micropores.

The boundary conditions at the top and bottom of the layer, $z = d$ and $z = -d_m$ are specified as follows

$$\begin{aligned}
V_i &= 0, \quad T = T_U, \quad \text{on } z = d, \\
U_3^f &= 0, \quad U_3^p = 0, \quad T^m = T_L, \quad \text{on } z = -d_m,
\end{aligned} \tag{3}$$

where T_U, T_L are constants with $T_L > T_U > 0$. Under these conditions (1) and (2) admit a steady conduction solution of form

$$\begin{aligned}
\bar{U}_i^f &= 0, \quad \bar{U}_i^p = 0, \quad \bar{V}_i = 0, \\
\bar{T} &= T_0 - (T_0 - T_U) \frac{z}{d}, \quad 0 \leq z \leq d, \\
\bar{T}^m &= T_0 - (T_L - T_0) \frac{z}{d_m}, \quad -d_m \leq z \leq 0,
\end{aligned} \tag{4}$$

where we have employed the fact that the temperature is continuous across the interface $z = 0$. To determine the constant T_0 we require the heat flux to be

continuous across the interface $z = 0$ and then

$$k_m \frac{d\bar{T}^m}{dz} = k_f \frac{d\bar{T}}{dz}, \quad \text{at } z = 0.$$

This yields T_0 as

$$T_0 = \frac{k_f T_U d_m + k_m T_L d}{dk_m + d_m k_f}. \quad (5)$$

3 Perturbation equations

As our goal is to study instability of the base solution (4) we now introduce perturbations to the variables $V_i, T, p^f, U_i^f, U_i^p, T^m, p^p$ as $u_i, \theta, \pi^f, u_i^f, u_i^p, \theta^m$ and π^p . We derive the perturbation equations for these variables from equations (1) and (2). However, it is convenient to present these in non-dimensional form with length scales d, d_m in the fluid and bidisperse porous layers, and with corresponding velocity scales U and U^m , although we here select $U = U^m$. The time scales are \mathcal{T} and \mathcal{T}^m where $\mathcal{T} = d^2/\nu$, with $\nu = \mu/\rho_0$ and we pick $\mathcal{T} = \mathcal{T}^m$. The pressure scale is $P = \mu U/d$. The temperature scales are

$$T^\# = \frac{U(T_0 - T_U)d(\rho_0 c_p)_f}{k_f}$$

and

$$T_m^\# = U^m(T_L - T_0) \frac{d_m(\rho_0 c_p)_f}{k_m}$$

and thus one finds

$$\frac{T^\#}{T_m^\#} = \left(\frac{k_m}{k_f}\right)^2 \hat{d}^2, \quad \frac{T_0 - T_U}{T_L - T_0} = \frac{k_m}{k_f} \hat{d}$$

where $\hat{d} = d/d_m$. It is convenient to introduce the notation

$$\hat{k} = \frac{k_f}{k_m}, \quad \hat{\kappa} = \frac{(\rho_0 c)_m}{(\rho_0 c)_f} \hat{k},$$

and to define the Prandtl number, Pr , and the porous Prandtl number, Pr_m , by

$$Pr = \frac{\nu}{\kappa} = \frac{\mu}{\rho_0} \frac{(\rho_0 c_p)_f}{k_f}, \quad Pr_m = \frac{\mu}{\rho_0} \frac{(\rho_0 c)_m}{k_m}$$

from which one may show $Pr_m = \hat{\kappa} Pr$.

The fluid and porous Rayleigh numbers Ra and Ra^m are defined by

$$Ra = \frac{\gamma g d^4 (T_0 - T_U)}{\kappa_f \nu}, \quad (6)$$

where $\kappa_f = k_f/(\rho_0 c_p)_f$, and

$$Ra_m = \gamma g K^f \frac{(T_L - T_0)}{d_m} \frac{d_m^2}{[k_m/(\rho_0 c)_f] \nu}, \quad (7)$$

from which one shows

$$Ra = \left(\frac{\hat{d}}{\hat{k}}\right)^2 \frac{Ra_m}{Da}$$

where Da is the Darcy number defined here as

$$Da = \frac{K_f}{\hat{d}^2}.$$

The relative permeability K_r is defined by $K_r = K_f/K_p$, and another useful non-dimensional variable is $\delta = \sqrt{K_p}/d_m$, from which we may see that $Da = K_r \delta^2 / \hat{d}^2$.

With the above non-dimensionalization one may show that the linearized fluid perturbation equations have form

$$\begin{aligned} u_{i,t} &= -\pi_{,i} + \Delta u_i + Rak_i \theta, \\ u_{i,i} &= 0, \\ Pr\theta_{,t} &= w + \Delta \theta \end{aligned} \tag{8}$$

where $w = u_3$ and these equations hold on $\mathbb{R}^2 \times \{z \in (0, 1)\} \times \{t > 0\}$ while the linearized bidispersive porous media equations have form

$$\begin{aligned} -u_i^f - \xi(u_i^f - u_i^p) - \pi_{,i}^f + Ra^m k_i \theta^m &= 0, \\ u_{i,i}^f &= 0, \\ -K_r u_i^p - \xi(u_i^p - u_i^f) - \pi_{,i}^p + Ra^m k_i \theta^m &= 0, \\ u_{i,i}^p &= 0, \\ \frac{Pr^m}{\hat{d}^2} \theta_{,t}^m &= w^f + w^p + \Delta \theta_m \end{aligned} \tag{9}$$

where $w^f = u_3^f$, $w^p = u_3^p$ and equations (9) hold on $\mathcal{R}^2 \times \{z_m \in (-1, 0)\} \times \{t > 0\}$. The non-dimensional momentum transfer interaction coefficient ξ is defined by $\xi = \zeta K_f / \mu$.

Equations (8) and (9) when reduced to the thermal convection instability problem essentially represent a twelfth order system of equations. We thus require twelve boundary conditions. In this work we employ a normal mode instability analysis and it is sufficient to require the following conditions

$$w = w' = \theta = 0, \quad \text{on } z = 1,$$

where $w' = \partial w / \partial z$. This corresponds to a fixed upper surface. Also,

$$w^f = w^p = \theta^m = 0, \quad \text{on } z = -1.$$

The remaining six boundary conditions come from considerations on the interface $z = 0$. At the microscopic level the velocity W in the fluid should be continuous across the interface with the actual velocity W^f in a macro pore and

with the actual velocity W^p in a micro pore. In dimensional form this requires at $z = 0$,

$$W = \frac{W^f}{\phi}, \quad \text{and} \quad W = \frac{W^p}{\epsilon(1-\phi)},$$

where w^f and w^p are the pore averaged values. Likewise the dimensional temperatures are continuous so

$$\theta = \theta_m, \quad \text{at} \quad z = 0.$$

In addition the normal component of heat flux $\mathbf{q} \cdot \mathbf{n}$ is continuous across $z = 0$. Two further conditions are needed and these arise by requiring continuity of normal stress, and by appealing to a combination of appropriate forms of the experimentally verified Beavers and Joseph [2] condition. Details of these boundary conditions are amplified below.

4 Instability analysis

The next step is to remove the pressure terms π, π^f and π^p from (8) and (9) and this we do by taking curl curl of equations (8)₁ and (9)_{1,3} and retaining the third component. This results in the system of equations

$$\begin{aligned} \sigma \Delta w &= \Delta^2 w + Ra \Delta^* \theta, \\ \sigma Pr \theta &= w + \Delta \theta, \end{aligned} \tag{10}$$

and

$$\begin{aligned} (1 + \xi) \Delta w^f - \xi \Delta w^p - Ra^m \Delta^* \theta^m &= 0, \\ (K_r + \xi) \Delta w^p - \xi \Delta w^f - Ra^m \Delta^* \theta^m &= 0, \\ \frac{\sigma_m Pr_m}{\hat{d}^2} \theta^m &= w^f + w^p + \Delta \theta^m, \end{aligned} \tag{11}$$

where we have represented time by $e^{\sigma t}$ in the fluid equations and by $\exp(\sigma_m t)$ in the bidisperse porous equations. The symbol Δ^* is the horizontal Laplacian. Equations (10) hold on $\mathbb{R}^2 \times (0, 1)$ while (11) hold on $\mathbb{R}^2 \times (-1, 0)$.

We next solve (11)_{1,2} in terms of Δw^f and Δw^p . We represent w and θ as $w = W(z)h(x, y)$, $\theta = \Theta(z)h(x, y)$, and $w^f = W^f(z)h^m(x, y)$, $w^p = W^p(z)h^m(x, y)$, $\theta_m = \Theta_m(z)h^m(x, y)$, where h and h_m are plan forms which tile the plane, cf. Chandrasekhar [10], pp. 43-52, and are typical of the hexagonal convection cell forms found in real life. The functions h and h_m satisfy the relations $\Delta^* h = -a^2 h$ and $\Delta^* h_m = -a_m^2 h_m$, for wavenumbers a and a_m . We reduce (10)₁ to two second order equations by setting $\Delta w = \chi$, and then we arrive at the following coupled system of equations to solve for the growth rate (eigenvalues) σ, σ_m ,

$$\begin{aligned} (D^2 - a^2)W - \chi &= 0, \\ (D^2 - a^2)\chi - Ra a^2 \Theta &= \sigma \chi, \\ (D^2 - a^2)\Theta + W &= Pr \sigma \Theta, \end{aligned} \tag{12}$$

on $z \in (0, 1)$, where $D = d/dz$, and

$$\begin{aligned} (D^2 - a_m^2)W^f + Ra_m a_m^2 \frac{(K_r + 2\xi)}{(K_r + \xi + \xi K_r)} \Theta_m &= 0, \\ (D^2 - a_m^2)W^p + Ra_m a_m^2 \frac{(1 + 2\xi)}{(K_r + \xi + \xi K_r)} \Theta_m &= 0, \\ (D^2 - a_m^2)\Theta_m + W^f + W^p &= \frac{Pr_m}{\hat{d}^2} \sigma_m \Theta_m, \end{aligned} \quad (13)$$

on $z_m \in (-1, 0)$.

The non-dimensional boundary conditions are

$$\begin{aligned} W = W' = \Theta = 0, \quad z = 1, \\ W^f = W^p = \Theta^m = 0, \quad z = -1, \end{aligned} \quad (14)$$

together with the non-dimensional interface conditions

$$\begin{aligned} W = \frac{W^p}{\epsilon(1 - \phi)}, \quad \frac{W = W^f}{\phi}, \quad z = 0, \\ \theta_m = \theta \left(\frac{k_m}{k_f} \right)^2 \hat{d}^2, \quad \frac{d\theta_m}{dz_m} = \frac{d\theta}{dz} \hat{d} \frac{k_m}{k_f}, \quad z = 0, \end{aligned} \quad (15)$$

where the latter two arise due to continuity of temperature, and continuity of heat flux.

For the remaining interface conditions we argue as follows.

In terms of the fluid and pore averaged velocities at the microscopic level, the Beavers and Joseph [2] condition may be applied separately to the macro and micro components to yield in dimensionless form

$$\frac{1}{d} \frac{\partial u_\beta}{\partial z} = \frac{\alpha_1}{\sqrt{K_f}} (u_\beta - u_\beta^f), \quad \beta = 1, 2, \quad (16)$$

and

$$\frac{1}{d} \frac{\partial u_\beta}{\partial z} = \frac{\alpha_2}{\sqrt{K_p}} (u_\beta - u_\beta^p), \quad \beta = 1, 2, \quad (17)$$

where α_1 and α_2 are experimentally determined constants. For a single porosity material Beavers and Joseph [2] write that “ α is a dimensionless quantity depending on the material parameters which characterize the structure of permeable material within the boundary region”. Our first approach is to take an averaged value of each of the conditions (16) and (17) and propose at the interface $z = 0$,

$$\frac{\partial u_\beta}{\partial z} = (A_1 + A_2)u_\beta - A_1 u_\beta^f - A_2 u_\beta^p, \quad \beta = 1, 2, \quad (18)$$

where

$$A_1 = \frac{\alpha_1 d}{2\sqrt{K_f}} \quad A_2 = \frac{\alpha_2 d}{2\sqrt{K_p}}. \quad (19)$$

We next differentiate (18) and employ the incompressibility conditions to derive the interface condition

$$w_{zz} = (A_1 + A_2)w_z - A_1 \hat{d}w_{z_m}^f - A_2 \hat{d}w_{z_m}^p \quad (20)$$

where the derivatives are with respect to z, z_m non-dimensional, $0 \leq z \leq 1$, $-1 \leq z_m \leq 0$.

We also consider an alternative procedure whereby we combine the Beavers and Joseph [2] conditions (16) and (17) in a manner which reflects the macro and micro contributions. Thus, define the constants c_1 and c_2 by

$$c_1 = \frac{\phi}{\phi + \epsilon(1 - \phi)}, \quad c_2 = \frac{\epsilon(1 - \phi)}{\phi + \epsilon(1 - \phi)}.$$

We now produce an equation of form (18) but where now

$$A_1 = c_1 \alpha_1 d / \sqrt{K_f} \quad A_2 = c_2 \alpha_2 d / \sqrt{K_p}. \quad (21)$$

We thus derive an equation of form (20) but with A_1 and A_2 as given here. The differences in employing (20) and the pore weighted version just discussed are considered in the numerical results section. For ease in understanding the numerical results where the effect of parameter variation upon the solution is considered we specifically write the two versions of (20) here as, equal splitting,

$$w_{zz} = \left(\frac{\alpha_1 d}{2\sqrt{K_f}} + \frac{\alpha_2 d}{2\sqrt{K_p}} \right) w_z - \frac{\alpha_1 d}{2\sqrt{K_f}} \hat{d}w_{z_m}^f - \frac{\alpha_2 d}{2\sqrt{K_p}} \hat{d}w_{z_m}^p \quad (22)$$

and pore weighted

$$w_{zz} = \left(\frac{c_1 \alpha_1 d}{\sqrt{K_f}} + \frac{c_2 \alpha_2 d}{\sqrt{K_p}} \right) w_z - \frac{c_1 \alpha_1 d}{\sqrt{K_f}} \hat{d}w_{z_m}^f - \frac{c_2 \alpha_2 d}{\sqrt{K_p}} \hat{d}w_{z_m}^p. \quad (23)$$

At the microscopic level, continuity of normal stress at the interface $z = 0$ requires

$$\pi^f = \pi - 2\mu w_z, \quad \text{for a macropore,}$$

and

$$\pi^p = \pi - 2\mu w_z, \quad \text{for a micropore.}$$

Our first continuity of normal stress interface condition is

$$\frac{\pi^f + \pi^p}{2} = \pi - 2\mu w_z, \quad \text{on } z = 0. \quad (24)$$

Equation (24) is differentiated with respect to x_α , $\alpha = 1, 2$, and one then employs the differential equations (8)_{1,2} and (9)₁₋₄ in the forms

$$\begin{aligned} \pi_{,\alpha} &= \Delta u_\alpha - \sigma u_\alpha, & u_{\alpha,\alpha} + w_{,z} &= 0, \\ \pi_{,\alpha}^f &= -u_\alpha^f - \xi(u_\alpha^f - u_\alpha^p), & u_{\alpha,\alpha}^f + w_{,z}^f &= 0, \\ \pi_{,\alpha}^p &= -K_r u_\alpha^p - \xi(u_\alpha^p - u_\alpha^f), & u_{\alpha,\alpha}^p + w_{,z}^p &= 0, \end{aligned} \quad (25)$$

to eliminate the pressure terms. The differentiated form of (24) is rewritten using (25) as

$$\frac{1}{2}(-u_\alpha^f - \xi[u_\alpha^f - u_\alpha^p] - Kr u_\alpha^p - \xi[u_\alpha^p - u_\alpha^f]) = \Delta u_\alpha - \sigma u_\alpha - 2\mu w_{,z\alpha}, \quad (26)$$

where $\alpha = 1, 2$. Note that in this case the ξ terms disappear. Now differentiate (26) for $\alpha = 1$ with respect to x and for $\alpha = 2$ with respect to y . This yields after summation to

$$\frac{1}{2}(-u_{\alpha,\alpha}^f - Kr u_{\alpha,\alpha}^p) = \Delta u_{\alpha,\alpha} - \sigma u_{\alpha,\alpha} - 2\mu w_{,z\alpha\alpha}.$$

Then use the incompressibility conditions to find

$$\frac{1}{2}(w_{,z}^f + Kr w_{,z}^p) = -\Delta w_{,z} + \sigma w_{,z} - 2\mu \Delta^* w_{,z} \quad (27)$$

where $\Delta^* = \partial^2/\partial x^2 + \partial^2/\partial y^2$. Equation (25)₃ allows one to determine the following non-dimensional interface condition

$$\frac{1}{2}(D_m w^f + Kr D_m w^p) = \frac{Da}{d} (\sigma Dw - D^3 w - 3\Delta^* Dw), \quad (28)$$

where $D = d/dz$, $z \in (0, 1)$, $D_m = d/dz_m$, $z_m \in (-1, 0)$.

Alternatively, one may employ a weighted form of (24) where we write

$$c_1 \pi^f + c_2 \pi^p = \pi - 2\mu w_z.$$

This then leads to a weighted form of (28). In deriving the weighted form the interaction terms involving ξ do not vanish. The precise forms are given in the next section.

Thus, the complete set of boundary conditions are (14), (15), together with (20) and (28), or the weighted equivalents of these latter two equations.

5 Numerical method

We solve equations (12) and (13) by a Chebyshev tau method, cf. Dongarra et al. [17], coupled with the QZ algorithm for a generalized matrix eigenvalue problem, cf. Moler and Stewart [37]. Equations (12) are transformed into the Chebyshev domain $(-1, 1)$ and equations (13) are likewise transformed into the same domain with the interface now being $z = -1$. The variables $W, \chi, \Theta, W^f, W^p$ and Θ^m are written as finite series of Chebyshev polynomials, e.g.

$$W = \sum_{i=0}^N W_i T_i(z),$$

for Fourier coefficients W_i . This yields a block matrix generalized eigenvalue problem of form $A\mathbf{x} = \sigma B\mathbf{x}$ for $6N \times 6N$ matrices A, B with B singular, where

$$\mathbf{x} = (\tilde{W}, \tilde{\chi}, \tilde{\Theta}, \tilde{W}^f, \tilde{W}^p, \tilde{\Theta}^m)$$

\tilde{W} etc., being the truncated versions of W , etc., i.e.

$$\tilde{W} = (W_0, \dots, W_N), \dots, \tilde{\Theta}^m = (\Theta_0^m, \dots, \Theta_N^m).$$

The boundary conditions are likewise expanded in Chebyshev polynomials and added as rows of the matrices A and B via a similar procedure to that explained in Dongarra et al. [17].

The complete set of boundary conditions on $z = 1$ or $z = -1$ are now

$$\begin{aligned} W = 0, \quad DW = 0, \quad \Theta = 0, \quad W^f = 0, \quad W^p = 0, \quad \Theta_m = 0, \quad z = 1, \\ W = \frac{W^f}{\phi}, \quad W = \frac{W^p}{\epsilon(1-\phi)}, \quad z = -1, \\ \Theta_m = \Theta \frac{\hat{d}^2}{\hat{k}^2}, \quad D_m \Theta_m + \frac{\hat{d}}{\hat{k}} D \Theta = 0, \quad z = -1, \\ A + a^2 W - 2(A_1 + A_2) DW \\ - 2A_2 \hat{d} D_m W^p - 2A_1 \hat{d} D_m W^f = 0, \quad z = -1, \end{aligned} \quad (29)$$

and

$$2DA - 4a^2 DW - \frac{\hat{d}}{Da} D_m W^f - \frac{K_r \hat{d}}{Da} D_m W^p = 2\sigma DW, \quad z = -1. \quad (30)$$

This is for the case (24) and (20) with A_1 and A_2 given by (19). When the weighted version of the Beavers - Joseph and continuity of normal stress conditions are employed then (29)₃ holds but with A_1 and A_2 given by (21). However, in the weighted case (30) should be replaced by

$$\begin{aligned} 2DA - 4a^2 DW - \frac{2\hat{d}}{Da} [c_1 + \xi(c_1 - c_2)] D_m W^f \\ - \frac{2\hat{d}}{Da} [K_r c_2 + \xi(c_2 - c_1)] D_m W^p = 2\sigma DW, \end{aligned} \quad (31)$$

where it is to be observed that the interaction terms involving ξ are present.

6 Numerical results

This section reports on numerical results for the critical Rayleigh number and critical wavenumber for the equations for thermal convection in a linearly viscous fluid overlying a bidisperse porous material. We choose parameter values appropriate to water being the working fluid and a bidisperse porous material being based upon a glass bead skeleton.

As this is the first calculation for this problem we restrict attention to $\alpha_1 = \alpha_2 = \alpha$ for the Beavers - Joseph constant. Since there are many parameters we believe this is justified. For numerical values of the many parameters we refer to Gentile and Straughan [22] who employed tabulated experimental values of

Hooman et al. [29], Imani and Hooman [30], Chen [13], Rees [43, 44] and Nield [39].

Beavers and Joseph [2] reported values of α for a single porosity material in the range 0.1 to 4. These values are for a granular aloxite material and for man made porous foams. In this work we concentrate on more granular materials and choose α values close to 0.1. The values reported in Gentile and Straughan [22] suggest we take relative permeabilities of

$$K_r = 25, 151.7, 263.16$$

and values for the non-dimensional momentum transfer coefficient in the group

$$\xi = 1.515 \times 10^{-2}, 2.347 \times 10^{-2}, 2.987 \times 10^{-2}, 0.1316.$$

We here choose to investigate the behaviour of the critical Ra_m and a_m values upon $K_r, \alpha, \xi, \phi, \epsilon$, and upon the equal splitting interface conditions of Beavers and Joseph and continuity of normal stress together with the analogous pore weighted interface conditions.

For core values using glass beads and water the thermal conductivities, densities and specific heats are taken from the internet version of Engineering Toolbox to yield $k_m, k_f, (\rho c)_m$ and $(\rho c)_f$. We also employ the parameter ranges in Gentile and Straughan [22] to find values for ξ, K_r and δ . In this way we obtain $Pr = 6, Pr_m = 0.75828, Da = 0.161278 \times 10^{-2}, \delta = 0.3279 \times 10^{-2}, \hat{k} = 0.16736, \phi = 0.3, \epsilon = 0.3, \alpha = 0.1, \xi = 0.02987, \hat{\kappa} = 0.12638, K_r = 25$, although specific values will be varied at appropriate points in our discussion. The nature of the onset of convective motion in all cases depends on \hat{d} , the depth of fluid layer to depth of porous layer. There is a critical value of \hat{d} such that when \hat{d} is below this value then convective motion commences in the porous layer whereas such motion is initiated in the fluid layer when \hat{d} is above the critical value. The critical \hat{d} value also depends strongly on the other parameters in the problem and this variation is examined in detail here.

The bimodal behaviour of the neutral curves is displayed in figures 1 and 2. Figure 1 shows that when $\hat{d} = 0.12$ the lowest minimum for Ra_m is at $a_m = 2.1$ and this corresponds to convection initiating in the porous layer, whereas when $\hat{d} = 0.13$ the lowest minimum for Ra_m is at $a_m = 17.0$ and this corresponds to convective motion initiating in the fluid layer. From table 1 we see that the critical value for \hat{d} corresponding to figure 1 is when $\hat{d}_{crit} \in (0.1260, 0.1261)$. Observe that from table 1 the wavenumber jumps from $a_m = 2.1$ to $a_m = 17.7$ as the initiation of convection switches from the porous layer to the fluid layer. Since a_m is inversely proportional to the aspect ratio of the convection cell this means that for a non-dimensional depth of porous layer of 1 the width of the cell changes from $2\pi/2.1$ to $2\pi/17.7$, i.e. from 2.99 to 0.355, or from wide cells in the porous layer to cells 8.42 times smaller in the fluid layer. Of course, the aspect ratio also depends on other parameters in the bidispersive porous medium. Figure 2 also displays a switch from convection in the porous layer to convection in the fluid layer, but now when \hat{d} is fixed. In this case the switch of convection is due to the macro porosity changing.

It is noticeable that the minima associated to the fluid are widely separated in figure 1 whereas in 2 it is the minima associated to the porous medium which display the greater variation. Since figure 2 is displaying changes in the porosity the larger variation in the “porous minimum” is to be expected.

Table 1 displays how the critical values of the porous Rayleigh number Ra_m and the critical values of the porous wavenumber a_m change as K_r is varied. Since we are effectively fixing K^f in our computations changing K_r corresponds to changing $1/K^p$. As K_r increases in table 1 from values of 1.5 through to 263.16 we see that Ra_m increases, both for the porous and fluid minima. This corresponds to the layered system becoming less easy to convect as $\Delta T = T_L - T_U$ increases. Since K_r increasing corresponds to K^p decreasing this means it is more difficult for the fluid to move in the micro pores and so we expect the system to be more stable. It is worth observing that in all our computations we have found that at criticality the growth rate σ is real.

From table 1 the porous wavenumber a_m increases by a factor of approximately 2.5 over the range of variation of K_r but the wavenumber corresponding to the fluid decreases from 24.4 or 26.1 to 9.3 or 8.3, respectively, depending on the value of \hat{d} . Thus, at the onset of convection when the motion is initiated in the porous layer increasing K_r decreases the cell aspect ratio whereas the opposite is true when the convective motion is initiated in the fluid layer. The quantitative value of this effect does demonstrate that the presence of the bidisperse layer is significant in both cell aspect ratio and whether convection will occur.

Table 2 displays how Ra_m and a_m change at criticality with variation in the Beavers - Joseph interface parameter. We find that increasing α decreases the value of Ra_m and also that of a_m . Since the coefficient α multiplies $u_\alpha - u_\alpha^{f,p}$ increasing its value has the effect of increasing the shear flow term $\partial u_\alpha / \partial z$ which is making the system more stable and increasing the convection cell aspect ratio.

Table 3 displays the effect of changing the momentum transfer coefficient ξ upon Ra_m and a_m . It is seen that a relative change of over 4 in ξ reduces both Ra_m and a_m , although the change is relatively small.

Table 4 demonstrates how the critical values of Ra_m and a_m are affected by changing the macro porosity ϕ and the micro porosity ϵ . For a fixed value of ϕ increasing ϵ leads to an increase in Ra_m and a_m for the convection initiation in the porous medium, while the values associated to initiation in the fluid part of the layer show little variation. This indicates that increasing ϵ for fixed ϕ helps to stabilize the fluid layer. This could be an important factor in any application which requires the fluid/porous layer to not convect.

Increasing ϕ for fixed ϵ decreases both Ra_m and a_m as might be expected since a larger macro porosity should mean convective motion is easier to commence. However, care must be taken in interpretation. The Rayleigh number Ra_m as defined in (7) may be rewritten as

$$Ra_m = \frac{\gamma g (T_L - T_U) d_m d^2}{\kappa_m \nu} \frac{Da}{(1 + \hat{d}/\hat{k})} \frac{(\rho c)_f}{(\rho c)_m}. \quad (32)$$

Clearly Ra_m has the correct structure but since $Da = K_f/d^2$ there is a direct dependence on the macro permeability K^f and it is widely believed that K^f depends strongly on ϕ . For example, for glass spheres Chen [13] uses the Carmen - Kozeny relation

$$K^f = \frac{d_s^2}{172.8} \frac{\phi^3}{(1-\phi)^2}$$

where d_s is the diameter of the glass beads. It is clear that Ra_m in (32) would then depend strongly on ϕ and in any application this would need to be taken into account.

We have calculated the necessary values of a_m even though they are not displayed in table 4. For the first set of values where $\phi = 0.5$ and $\epsilon = 0.2, \dots, 0.6$, convection always initiates in the porous zone, and a_m takes values 1.4, 1.8, 2.0, 2.1 and 2.2, respectively, while $a_m^{(2)}$ has values 18.6 and 18.7 four times. This means lowering the micro porosity increases the width of the convection cells. It is useful to compare this with the case of a single porosity material as studied in Straughan [49]. Figure 7 and table VII of that work are appropriate as $\phi = 0.5$ there. However, it is difficult to compare directly since the meaning of terms is different, for example, here $\delta = \sqrt{K_p}/d_m$ whereas in Straughan [49], $\delta = \sqrt{K}/d_m$ with K being the permeability in the single porosity medium. Nevertheless, the case in Straughan [49] demonstrates convection initiates strongly in the porous region. The single porosity case is formally achieved for equations (8) and (9) by taking $\xi = 0$ and $K_r = 1$, although this is a formal calculation since $\epsilon \rightarrow 0$ needs a careful treatment of interface conditions. Although if we take $\xi = 0$ and $K_r = 1$ and compute $a_m, Ra_m, a_m^{(2)}$ and $Ra_m^{(2)}$ we find for $\hat{d} = 0.08$, $a_m = 1.0$, $Ra_m = 3.183$, $a_m^{(2)} = 27.6$, $Ra_m^{(2)} = 5.124$ whereas when $\hat{d} = 0.09$, $a_m = 0.7$, $Ra_m = 2.695$, $a_m^{(2)} = 23.6$, $Ra_m^{(2)} = 3.080$. If these values are compared with corresponding values in table 1, for $K_r = 1.5$ and table 4 then we see that as ϵ decreases Ra_m decreases and the layer system becomes less stable. This is important because for some applications one requires the layer to not convect and so the presence of a bidisperse porous medium is highly beneficial. For example, in experiments with a solar pond Wang et al. [58] found that the presence of a porous layer stabilizes the pond and increases efficiency, but, additionally the presence of a bidisperse porous material further stabilizes and increases efficiency. Of course, our model does not describe a solar pond where one must also account for a salt distribution and different boundary conditions due to solar radiation heating. However, we do believe it is very interesting that our model does predict the presence of a bidisperse porous layer could be very beneficial in applications.

Finally tables 5 and 6 show the variation in the values of Ra_m depending on whether the Beavers - Joseph and continuity of normal stress conditions employ the equally split (ES) value of 0.5 or the pore weighted (PW) values. For the K_r and α values selected here the variation is relatively small, but not totally insignificant. It would be useful to have experimental results to compare with in order to assess which class of interface conditions is preferable.

7 Conclusions

We have formulated equations for thermal convection in a fluid layer which overlies a layer of bidisperse (or double porosity) porous medium saturated by the same fluid. The macro and micro porosities ϕ and ϵ and the analogous macro and micro permeabilities K^f and K^p are explicitly included and play a major role in the model along with the depth of the fluid layer d and the depth of the porous layer d_m . The interface conditions between the fluid and porous medium are very important and we have adopted two approaches. One is to adopt an equal weighting to both the macro and micro phases while the other approach employs a pore weighted average reflecting the relative porosities ϕ and ϵ .

We suggest a variant of the Beavers and Joseph [2] interface condition which holds when the porous medium is one of bidisperse type. In general, this allows for two Beavers - Joseph interface coefficients α_1 and α_2 corresponding to the macro and micro phases. In our numerical results we assume $\alpha_1 = \alpha_2$ although in specific applications α_1 may need to be different from α_2 and our model allows for this.

Our numerical results show that the bidisperse porous medium is very different from the single porous medium case in that the coefficients of the double porosity material do have a strong effect on convective instability. Since the two layer convection problem with a fluid overlying a bidisperse porous medium does have serious application to renewable energy generation, see e.g. Wang et al. [58, 59], we believe the current work is very useful. Of course, two layer convection with a single porosity medium already has many parameters, see e.g. Chen [13], Chen and Chen [14, 15, 16], Straughan [48, 49], while convection in a single bidisperse layer likewise involves many parameters. The combined problem is necessarily complicated and, therefore, involves a lot of parameters. Future work will apply this theory to specific renewable energy situations.

Conflict of interest statement. This work does not have any conflicts of interest.

Funding. The work of BS was supported by an Emeritus Fellowship of the Leverhulme Trust, EM-2019-022/9. PD acknowledges partial support by the DFG through project 441523275/SPP225.

References

- [1] A. J. Badday and A. J. Harfash. Chemical reaction effect on convection in bidisperse porous medium. *Transport in Porous Media*, 137:381–397, 2021.
- [2] G. S. Beavers and D. D. Joseph. Boundary conditions at a naturally permeable wall. *J. Fluid Mech.*, 30:197–207, 1967.

- [3] F. Capone and R. De Luca. The effect of the Vadasz number on the onset of thermal convection in rotating bidispersive porous media. *Fluids*, 5: 5040173, 2020.
- [4] F. Capone and G. Massa. The effects of Vadasz term, anisotropy and rotation on bidispersive convection. *Int. J. Nonlinear Mech.*, 135:103749, 2021.
- [5] F. Capone, R. De Luca, and M. Gentile. Thermal convection in rotating anisotropic porous layers. *Mechanics Res. Comm.*, 110:103601, 2020.
- [6] F. Capone, R. De Luca, and M. Gentile. Coriolis effect on thermal convection in a rotating bidispersive porous layer. *Proc. Roy. Soc. London A*, 476:20190875, 2020.
- [7] F. Capone, R. De Luca, and G. Massa. Effect of anisotropy on the onset of convection in rotating bidispersive Brinkman porous media. *Acta Mech.*, 232:3393–3406, 2021.
- [8] M. Carr and B. Straughan. Penetrative convection in a fluid overlying a porous layer. *Advances in Water Resources*, 26:263–276, 2003.
- [9] H. A. Chaloob, A. J. Harfash, and A. J. Harfash. Bidispersive thermal convection with relatively large macropores and generalized velocity and temperature boundary conditions. *Phys. Fluids*, 33:014105, 2021.
- [10] S. Chandrasekhar. *Hydrodynamic and hydromagnetic stability*. Dover, New York, 1981.
- [11] M. H. Chang, F. Chen, and B. Straughan. Instability of Poiseuille flow in a fluid layer overlying a porous layer. *J. Fluid Mech.*, 564:287–303, 2006.
- [12] T. Y. Chang, F. Chen, and M. H. Chang. Stability of plane Poiseuille - Couette flow in a fluid layer overlying a porous layer. *J. Fluid Mech.*, 826: 376–395, 2017.
- [13] F. Chen. Throughflow effects on convective instability in superposed fluid and porous layers. *J. Fluid Mech.*, 231:113–133, 1991.
- [14] F. Chen and C. F. Chen. Onset of finger convection in a horizontal porous layer underlying a fluid layer. *J. Heat Transfer*, 3:403–409, 1988.
- [15] F. Chen and C. F. Chen. Experimental investigation of convective stability in a superposed fluid and porous layer when heated from below. *J. Fluid Mech.*, 207:311–321, 1989.
- [16] F. Chen and C. F. Chen. Convection in superposed fluid and porous layers. *J. Fluid Mech.*, 234:97–119, 1992.

- [17] J. J. Dongarra, B. Straughan, and D. W. Walker. Chebyshev tau - QZ algorithm methods for calculating spectra of hydrodynamic stability problems. *Appl. Numer. Math.*, 22:399–435, 1996.
- [18] P. Falsaperla, G. Mulone, and B. Straughan. Bidispersive inclined convection. *Proc. Roy. Soc. London A*, 472:20160480, 2016.
- [19] F. Franchi, R. Nibbi, and B. Straughan. Continuous dependence on modelling for temperature dependent bidispersive flow. *Proc. Roy. Soc. London A*, 473:20170485, 2017.
- [20] M. Gentile and B. Straughan. Bidispersive thermal convection. *Int. J. Heat Mass Transfer*, 114:837–840, 2017.
- [21] M. Gentile and B. Straughan. Bidispersive vertical convection. *Proc. Roy. Soc. A*, 473:20170481, 2017.
- [22] M. Gentile and B. Straughan. Bidispersive thermal convection with relatively large macropores. *J. Fluid Mech.*, 898:A14, 2020.
- [23] D. Z. Han, Q. Wang, and X. M. Wang. Dynamic transitions and bifurcations for thermal convection in the superposed free flow and porous media. *Physica D*, 414:132687, 2020.
- [24] Y. Hibi. Modelling variable density flow in subsurface and surface water in the vicinity of the boundary between a surface water - atmosphere system and the subsurface. *J. Contaminant Hydrology*, 234:103688, 2020.
- [25] Y. Hibi and A. Tomigashi. Evaluation of a coupled model for numerical simulation of a multiphase flow system in a porous medium and a surface fluid. *J. Contaminant Hydrology*, 180:34–55, 2015.
- [26] A. A. Hill and B. Straughan. Poiseuille flow of a fluid layer overlying a porous layer. *J. Fluid Mech.*, 603:137–149, 2008.
- [27] A. A. Hill and B. Straughan. Global stability for thermal convection in a fluid overlying a highly porous material. *Proc. Roy. Soc. London A*, 465:207–217, 2009.
- [28] A. A. Hill and B. Straughan. Poiseuille flow in a fluid overlying a highly porous material. *Adv. Water Resources*, 32:1609–1614, 2009.
- [29] K. Hooman, E. Sauret, and M. Dahari. Theoretical modelling of momentum transfer function of bi-disperse porous media. *Appl. Thermal Engng.*, 75:867–870, 2015.
- [30] G. Imani and K. Hooman. Lattice boltzmann pore scale simulation of natural convection in a differentially heated enclosure filled with a detached or attached bidisperse porous medium. *Trans. Porous Media*, 116:91–113, 2017.

- [31] Y. Li, S. Xiao, and Y. Lin. Continuous dependence for the Brinkman - Forchheimer fluid interacting with a Darcy fluid in a bounded domain. *Math. Comp. Simulation*, 150:66–82, 2018.
- [32] Y. Li, X. Chen, and J. Shi. Structural stability in resonant penetrative convection in a Brinkman - Forchheimer fluid interfacing with a Darcy fluid. *Appl. Math. Optimization*, 85:<https://doi.org/10.1007/s00245-021-09791-7>, 2021.
- [33] Y. Li, S. Zhang, and C. Lin. Structural stability for the Brinkman equations interfacing with Darcy equations in a bounded domain. *Boundary Value Problems*, 27:<https://doi.org/10.1186/s13661-021-01501-0>, 2021.
- [34] W. Q. Lyu and X. M. Wang. Stokes - Darcy system, small Darcy number behaviour and related interfacial conditions. *J. Fluid Mech.*, 922:A4, 2021.
- [35] M. McCurdy, M. N. Moore, and X. Wang. Convection in a coupled free flow - porous media system. *SIAM J. Appl. Math.*, 79:2313–2338, 2019.
- [36] G. McKay and B. Straughan. Patterned ground formation under water. *Continuum Mech. Thermodyn.*, 5:145–162, 1993.
- [37] C. B. Moler and G. W. Stewart. An algorithm for the generalized matrix eigenvalue problem $Ax = \lambda Bx$. Technical report, Univ. Texas at Austin, 1971.
- [38] D. A. Nield. Onset of convection in a fluid layer overlying a layer of porous medium. *J. Fluid Mech*, 81:513–522, 1977.
- [39] D. A. Nield. Modelling fluid flow and heat transfer in a saturated porous medium. *J. Appl. Math. Decis. Sci.*, 81:165–173, 1977.
- [40] D. A. Nield and A. V. Kuznetsov. The onset of convection in a bidisperse of porous medium. *Int. J. Heat Mass Transfer*, 49:3068–3074, 2006.
- [41] L. E. Payne and B. Straughan. Analysis of the boundary condition at the interface between a viscous fluid and a porous medium and related modelling questions. *J. Math. Pures Appl.*, 77:317–354, 1998.
- [42] R. Ponalagusamy and R. Manchi. Mathematical study on two - fluid model for flow of K-L fluid in a stenosed artery with porous wall. *SN Applied Sciences*, 3:508, 2021.
- [43] D. A. S. Rees. Microscopic modelling of the two - temperature model for conduction in heterogeneous media: three - dimensional media. In *Proceedings of the fourth International Conference on Applications of Porous Media*, volume 13, pages 125–143, Istanbul, 2009. ICAPM.
- [44] D. A. S. Rees. Microscopic modelling of the two - temperature model for conduction in heterogeneous media. *J. Porous Media*, 13:125–143, 2010.

- [45] A. Samanta. Linear stability of a plane Couette - Poiseuille flow overlying a porous layer. *Int. J. Multiphase Flow*, 123:103160, 2020.
- [46] S. Saravanan and S. Vigneshwaran. Centrifugal filtration convection in bidisperse media. *Phys. Fluids*, 32:084109, 2020.
- [47] B. D. Sharma and P. K. Yadav. A two - layer mathematical model of blood flow in porous constricted blood vessels. *Transport in Porous Media*, 120: 239–254, 2017.
- [48] B. Straughan. Surface - tension - driven convection in a fluid overlying a porous layer. *J. Computational Phys.*, 170:320–337, 2001.
- [49] B. Straughan. Effect of property variation and modelling on convection in a fluid overlying a porous layer. *Int. J. Numer. Anal. Meth. Geomech.*, 26: 75–97, 2002.
- [50] B. Straughan. *Stability, and wave motion in porous media*, volume 165 of *Appl. Math. Sci.* Springer, New York, 2008.
- [51] B. Straughan. *Mathematical aspects of multi-porosity continua*, volume 38 of *Advances in Mechanics and Mathematics Series.* Springer, Cham, Switzerland, 2017.
- [52] B. Straughan. Horizontally isotropic bidispersive thermal convection. *Proc. Roy. Soc. London A*, 474:20180018, 2018.
- [53] B. Straughan. Anisotropic bidispersive convection. *Proc. Roy. Soc. London A*, 475:20190206, 2019.
- [54] B. Straughan. Horizontally isotropic double porosity convection. *Proc. Roy. Soc. London A*, 475:20180672, 2019.
- [55] A. Tiwari, P. D. Shah, and S. S. Chauhan. Solute dispersion in two - fluid flowing through porous tubes with a porous layer near the absorbibg wall: Model for dispersion phenomenon in microvessels. *Int. J. Multiphase Flow*, 131:103380, 2020.
- [56] K. Tsiberkin. Porosity effect on the linear stability of flow overlying a porous medium. *European Phys. J.*, 43:34, 2020.
- [57] S. A. Wajihah and D. S. Sankar. Effects of porosity in four - layared nonlinear blood rheology in constricted narrow arteries with clinical applications. *Computer Methods and Programs in Biomedicine*, 199:–, 2021.
- [58] H. Wang, X. L. Yu, F. Shen, and L. Zhang. A laboratory experimental study on effect of porous medium on salt diffusion of salt gradient solar pond. *Solar Energy*, 122:630–639, 2015.

- [59] H. Wang, L. G. Zhang, and Y. Y. Mei. Investigation on the exergy performance of salt gradient solar ponds with porous media. *Int. J. Exergy*, 25: 34–53, 2018.
- [60] C. Yin, C. W. Wang, and S. W. Wang. Thermal instability of a viscoelastic fluid in a fluid - porous system with a plane Poiseuille flow. *Appl. Math. Mech.*, 41:1631–1650, 2020.

Kr	\hat{d}	a_m	Ra_m	$a_m^{(2)}$	$Ra_m^{(2)}$
1.5	0.08	1.2	4.221	28.1	7.755
1.5	0.09	1.2	3.986	24.4	4.765
1.5	0.1	1.0	3.963	21.2	3.014
5	0.1	1.6	9.030	22.5	10.621
5	0.11	1.6	8.746	20.1	7.172
10	0.11	1.8	13.901	20.4	14.604
10	0.12	1.8	13.515	18.4	10.193
20	0.12	2.0	19.589	18.7	20.734
20	0.13	2.0	19.128	17.0	14.852
25	0.12	2.1	21.474	18.7	26.015
25	0.1260	2.1	21.178	17.7	21.276
25	0.1261	2.1	21.173	17.7	21.206
25	0.13	2.1	20.991	17.0	18.671
151.7	0.17	2.5	28.572	12.2	36.445
151.7	0.18	2.5	28.147	11.2	27.910
263.16	0.20	2.6	28.423	9.3	29.038
263.16	0.21	2.7	27.243	8.3	22.277

Table 1: The minimum values of the porous Rayleigh number and corresponding wavenumber for the first minimum, Ra_m, a_m , and the second minimum, $Ra_m^{(2)}, a_m^{(2)}$, for indicated values of Kr . Here, $Pr = 6$, $Pr_m = 0.75828$, $\delta = 0.003279$, $\hat{k} = 0.16736$, $\phi = 0.3$, $\epsilon = 0.3$, $\alpha = 0.1$, $\xi = 0.02987$, $\hat{\kappa} = 0.12638$. The \hat{d} values are shown in the table.

α	\hat{d}	a_m	Ra_m	$a_m^{(2)}$	$Ra_m^{(2)}$
0.1	0.12	2.1	21.474	18.7	26.014
0.105	0.12	2.1	21.355	18.6	25.630
0.11	0.12	2.0	21.201	18.4	25.224
0.115	0.12	2.0	20.971	18.2	24.793
0.12	0.12	1.9	20.621	18.0	24.333
0.125	0.12	1.6	19.944	17.7	23.842
0.125	0.125	1.5	19.787	16.7	19.887
0.125	0.126	1.5	19.750	16.5	19.184
0.1	0.13	2.1	20.991	17.0	18.670
0.11	0.13	2.0	20.868	16.6	17.939
0.12	0.13	1.8	20.492	16.1	17.097

Table 2: The minimum values of the porous Rayleigh number and corresponding wavenumber for the first minimum, Ra_m, a_m , and the second minimum, $Ra_m^{(2)}, a_m^{(2)}$, for indicated values of the Beavers - Joseph parameter α . Here, $Pr = 6$, $Pr_m = 0.75828$, $\delta = 0.003279$, $\hat{k} = 0.16736$, $\phi = 0.3$, $\epsilon = 0.3$, $\xi = 0.02987$, $\hat{\kappa} = 0.12638$, $Kr = 25$. The \hat{d} values are shown in the table.

ξ	\hat{d}	a_m	Ra_m	$a_m^{(2)}$	$Ra_m^{(2)}$
0.1316	0.12	2.1	22.590	18.7	26.023
0.1316	0.1245	2.1	22.345	17.9	22.367
0.1316	0.1246	2.1	22.339	17.9	22.293
0.1316	0.125	2.1	22.318	17.9	21.999
0.1316	0.13	2.1	22.062	17.0	18.676
0.02987	0.12	2.1	21.474	18.7	26.015
0.02987	0.125	2.1	21.226	17.9	21.992
0.02987	0.1261	2.1	21.173	17.7	21.206
0.02987	0.1262	2.1	21.168	17.7	21.137
0.02987	0.13	2.1	20.991	17.0	18.671

Table 3: The minimum values of the porous Rayleigh number and corresponding wavenumber for the first minimum, Ra_m, a_m , and the second minimum, $Ra_m^{(2)}, a_m^{(2)}$, for indicated values of the non-dimensional momentum transfer coefficient ξ . Here, $Pr = 6$, $Pr_m = 0.75828$, $\delta = 0.003279$, $\hat{k} = 0.16736$, $\phi = 0.3$, $\epsilon = 0.3$, $\hat{\kappa} = 0.12638$, $K_r = 25$, $\alpha = 0.1$. The \hat{d} values are shown in the table.

ϕ	ϵ	\hat{d}	a_m	Ra_m	$a_m^{(2)}$	$Ra_m^{(2)}$
0.5	0.2	0.12	1.4	12.310	18.6	24.010
0.5	0.3	0.12	1.8	17.210	18.7	25.239
0.5	0.4	0.12	2.0	19.782	18.7	25.994
0.5	0.5	0.12	2.1	21.394	18.7	26.503
0.5	0.6	0.12	2.2	22.495	18.7	26.871
0.2	0.5	0.12	2.4	25.195	18.7	27.311
0.3	0.5	0.12	2.3	24.232	18.7	27.104
0.4	0.5	0.12	2.2	23.008	18.7	26.843
0.6	0.5	0.12	2.0	19.197	18.7	26.043
0.3	0.3	0.12	2.1	21.474	18.7	26.015
0.3	0.3	0.1260	2.1	21.178	17.7	21.276
0.3	0.3	0.1261	2.1	21.173	17.7	21.206
0.3	0.3	0.13	2.1	20.991	17.0	18.671
0.5	0.2	0.14	1.3	11.692	15.6	12.909
0.5	0.2	0.1436	1.3	11.595	15.1	11.604
0.5	0.2	0.1437	1.3	11.593	15.1	11.570
0.5	0.2	0.15	1.3	11.439	14.2	9.630
0.3	0.5	0.12	2.3	24.232	18.7	27.104
0.3	0.5	0.1234	2.3	24.054	18.1	24.097
0.3	0.5	0.1235	2.3	24.049	18.1	24.014
0.3	0.5	0.13	2.3	23.703	17.0	19.296

Table 4: The minimum values of the porous Rayleigh number and corresponding wavenumber for the first minimum, Ra_m, a_m , and the second minimum, $Ra_m^{(2)}, a_m^{(2)}$, for indicated values of the macro porosity ϕ and micro porosity ϵ . $Pr = 6$, $Pr_m = 0.75828$, $\delta = 0.003279$, $\hat{k} = 0.16736$, $\xi = 0.02987$, $\hat{\kappa} = 0.12638$, $K_r = 25$, $\alpha = 0.1$. The \hat{d} values are shown in the table.

K_r	\hat{d}	$Ra_m(\text{ES})$	$Ra_m(\text{PW})$	$Ra_m^{(2)}(\text{ES})$	$Ra_m^{(2)}(\text{PW})$
20	0.12	19.589	18.199	20.734	20.997
20	0.13	19.128	17.666	14.852	15.216
25	0.12	21.474	20.132	26.015	26.310
25	0.13	20.991	19.539	18.671	19.103
151.7	0.17	28.572	28.048	36.445	39.233
151.7	0.18	28.147	27.632	27.910	30.664
151.7	0.19		27.113		24.152
263.16	0.19	29.013		37.655	
263.16	0.20	28.423	28.340	29.038	33.579
263.16	0.21	27.243	27.790	22.277	26.821

Table 5: The minimum values of the porous Rayleigh number and corresponding wavenumber for the first minimum, Ra_m , and the second minimum, $Ra_m^{(2)}$, for a comparison between the equally split (ES) and pore weighted (PW) versions of the Beavers - Joseph interface condition, and the continuity of normal stress at the interface. Here $Pr = 6$, $Pr_m = 0.75828$, $\delta = 0.003279$, $\hat{k} = 0.16736$, $\phi = 0.3$, $\epsilon = 0.3$, $\hat{\kappa} = 0.12638$, $\xi = 0.02987$, $\alpha = 0.1$. The \hat{d} , K_r values are shown in the table.

α	\hat{d}	$Ra_m(\text{ES})$	$Ra_m(\text{PW})$	$Ra_m^{(2)}(\text{ES})$	$Ra_m^{(2)}(\text{PW})$
0.1	0.12	21.474	20.132	26.014	26.310
0.105	0.12	21.355	20.018	25.630	26.034
0.11	0.12	21.201	19.867	25.224	25.745
0.115	0.12	20.971	19.681	24.793	25.442
0.12	0.12	20.621	19.442	24.333	25.123
0.125	0.12	19.944	19.115	23.842	24.788
0.13	0.12		18.608		24.434
0.135	0.12		17.659		24.059
0.1	0.13	20.991	19.539	18.670	19.103
0.11	0.13	20.868	19.372	17.939	18.584
0.12	0.13	20.492	19.075	17.097	18.005
0.13	0.13		18.352		17.352

Table 6: The minimum values of the porous Rayleigh number and corresponding wavenumber for the first minimum, Ra_m , and the second minimum, $Ra_m^{(2)}$, for a comparison between the equally split (ES) and pore weighted (PW) versions of the Beavers - Joseph interface condition, and the continuity of normal stress at the interface. Here $Pr = 6$, $Pr_m = 0.75828$, $\delta = 0.003279$, $\hat{k} = 0.16736$, $\phi = 0.3$, $\epsilon = 0.3$, $\hat{\kappa} = 0.12638$, $\xi = 0.02987$, $K_r = 25$. The \hat{d} , α values are shown in the table.

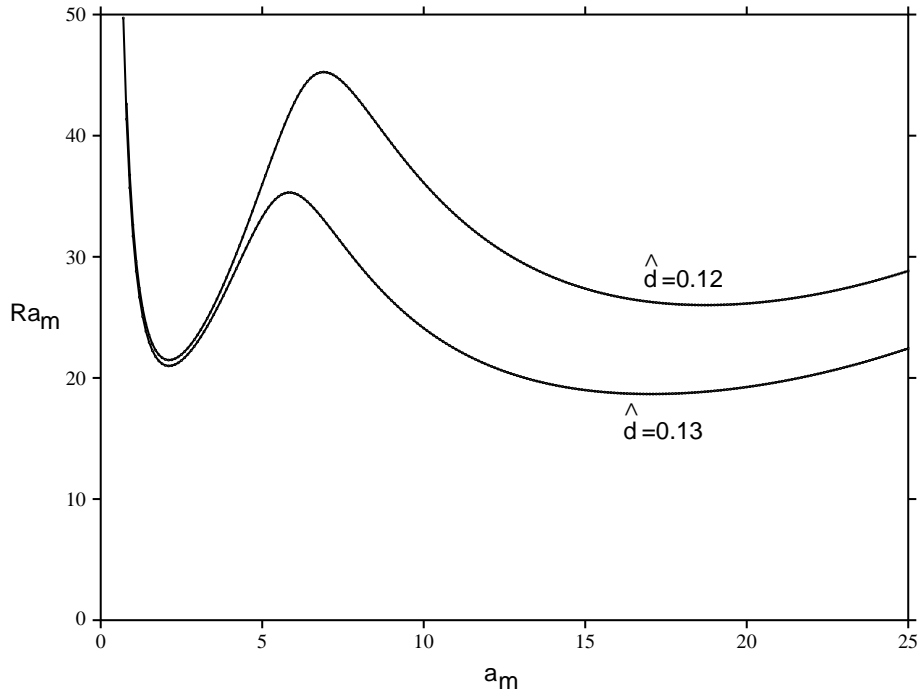


Figure 1: Graph of Ra_m vs. a_m . Here, $\delta = 0.003279$, $\hat{k} = 0.16736$, $\phi = 0.3$, $\epsilon = 0.3$, $\alpha = 0.1$, $\xi = 0.02987$, $\hat{\kappa} = 0.12638$, $Pr = 6$, $K_r = 25$. The minimum values on the $\hat{d} = 0.12$ curve are at $a_m = 2.1$, $Ra_m = 21.474$ and $a_m = 18.7$, $Ra_m = 26.015$, on the $\hat{d} = 0.13$ curve they are $a_m = 2.1$, $Ra_m = 20.991$ and $a_m = 17.0$, $Ra_m = 18.671$. The instability when $\hat{d} = 0.12$ initiates in the porous medium, whereas when $\hat{d} = 0.13$ it initiates in the fluid.

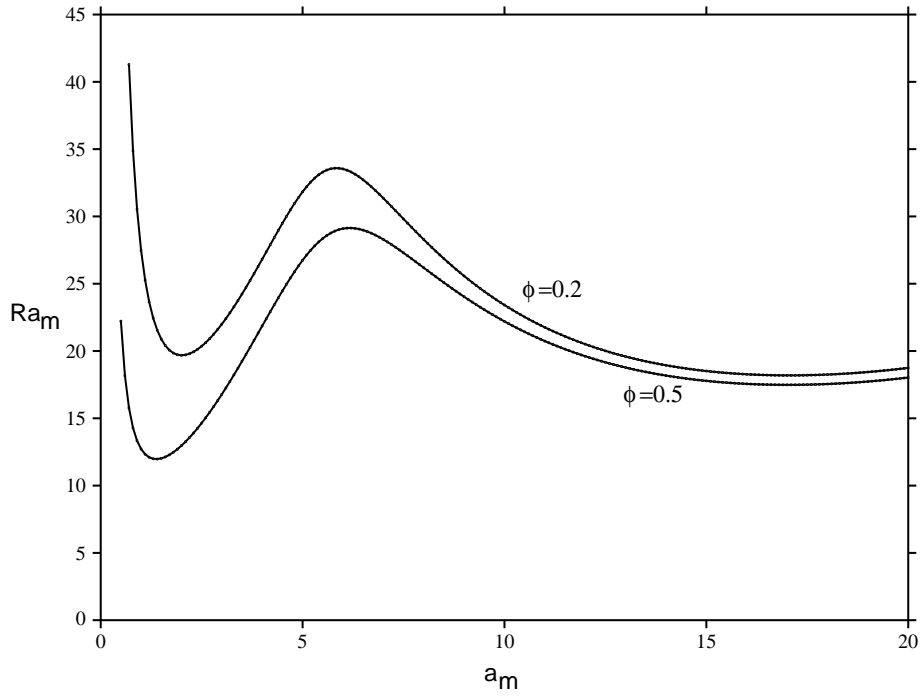


Figure 2: Graph of Ra_m vs. a_m . Here, $\delta = 0.003279$, $\hat{k} = 0.16736$, $\hat{d} = 0.13$, $\epsilon = 0.2$, $\alpha = 0.1$, $\xi = 0.02987$, $\hat{\kappa} = 0.12638$, $Pr = 6$, $K_r = 25$. The minimum values on the $\phi = 0.2$ curve are at $a_m = 2.0$, $Ra_m = 19.683$ and $a_m = 17.1$, $Ra_m = 18.191$, on the $\phi = 0.5$ curve they are $a_m = 1.4$, $Ra_m = 11.973$ and $a_m = 17.0$, $Ra_m = 17.486$. The instability when $\phi = 0.5$ initiates in the porous medium, whereas when $\phi = 0.2$ it initiates in the fluid.